ELSEVIER

Chemical Engineering Journal 128 (2007) 59–67

Chemical Engineering Journal

www.elsevier.com/locate/cej

Sewage sludge as a single precursor for development of composite adsorbents/catalysts

Mykola Seredych, Teresa J. Bandosz *

Department of Chemistry, The City College of New York, 138th Street and Convent Avenue, New York, NY 10031, United States

Received 23 January 2006; received in revised form 12 February 2006; accepted 27 June 2006

Abstract

New York City origin sewage sludge was pyrolyzed and converted into adsorbents. Pyrolysis conditions were modified in order to evaluate the development of catalytic surface towards hydrogen sulfide oxidation. The holding time ranged from 0.5 h to 2 h and the final temperature was 650 °C, 800 °C and 950 °C. The resulting materials were characterized using adsorption of nitrogen (surface area and pore volume), thermal analysis, X-ray diffractions, XRF, SEM-EDX, TEM and pH measurements. On these materials adsorption/oxidation of hydrogen sulfide from moist air was carried out and the products of the surface oxidation were evaluated. The results indicated development of catalytic surface with an increase in pyrolysis temperature and holding time. As a result of solid state high temperature reactions between main components of sewage sludge, mainly iron, zinc, copper, phosphorus, silica and alumina, new mineral phases are formed which are very active in the oxidation process. Moreover, the presence of catalytic metals and organic vapors results in formation of carbon nanotubes on the surface of sewage sludge derived adsorbents as a result of self imposed chemical vapor deposition process.

Keywords: Sewage sludge; Pyrolysis; Hydrogen sulfide; Reactive adsorption; Mineralization

1. Introduction

Recently many efforts have been focused on composite materials because of the possibility of their multifunctional applications. Mixing materials or creating their nanoscale assemblies very often leads to the synergetic effect in such processes as catalysis, gas storage, or drug delivery mechanisms [1]. The process involved in formation of nanocomposites are often time consuming and material demanding which ultimately increase their cost.

Interesting route of developing composite materials is based on utilization of wastes, such a polystyrene [2], clays exposed to heavy metal adsorption [3], or waste clays applied for removal of organic compounds in food production process (from vegetables oil) [4]. Also fly ash [5] or ash produced in burning fossil fuel [6], mainly coal, found interesting applications in composite materials.

During the last few years research in our laboratory has been focused on development of sewage sludge based adsorbents for desulfurization from gas phase [7–13]. It was shown that materials, which are the mixtures of inorganic oxides such as calcium, magnesium iron, copper, and carbon phase are excellent adsorbents for H_2S removal form moist air. This happens owing to a high dispersion of calcium species, which provide basic pH necessary for dissociation of hydrogen sulfide followed by oxidation of HS^- ions by active oxygen. Iron, on the other hand, activates oxygen and takes part in the electron transfer process (Fe^{3+}/Fe^{2+}). The presence of carbonaceous phase, even nonmicroporous [11] contributes to the dispersion of a sludge-based catalytic phase and provides space for storage of an oxidation product, elemental sulfur. On the other hand, presence of microporosity in the carbonaceous phase increases the adsorption capacity providing more space for sulfur [12]. The disadvantage here lies in an increase in the selectivity of H_2SO_4 formation via oxidation of sulfur radicals, located in small pores and separated from each other, to SO_2 [13]. A challenge in preparation of this kind of catalysts is that the high capacity for H_2S removal is achieved only when the carbon and inorganic phases are mixed at certain proportions [11,12]. Contrary to the elaborated technology used for production of catalytic carbon Midas® [14], the sewage sludge itself, as received, is a mixture of valuable active ingredients.

* Corresponding author. Tel.: +1 212 650 6017; fax: +1 212 650 6107.
E-mail address: tbandosz@ccny.cuny.edu (T.J. Bandosz).

1385-8947/$ – see front matter © 2006 Elsevier B.V. All rights reserved.
doi:10.1016/j.cej.2006.06.025

Mixing sewage sludge with spent mineral oil resulted in 20% higher capacity for H_2S removal than that obtained on the material derived from unmodified sludge. Some details about both types of adsorbents were described elsewhere [15]. The differences in the performances were attributed to the subtle changes in an organic phase, since the general composition of the inorganic phase seemed not to be affected.

The objective of this paper is to demonstrate a unique nanostructure and chemistry of sewage sludge derived adsorbents and its effect on the catalytic performance. As examples the materials carbonized between 650 °C and 950 °C were chosen as media on whose surface reactive adsorption of hydrogen sulfide occurs. The development of a catalytic surface is presented not only as a function of pyrolysis temperature but also of pyrolysis time. Both these factors were found as crucial towards "thermal activation" of sewage sludge derived materials.

2. Experimental

2.1. Materials

New York City dewatered sewage sludge was dried at 120 °C to constant mass and then pyrolyzed in a horizontal furnace in nitrogen atmosphere with 10°/min heating rate and nitrogen flow 100 mL/min. Holding time was 0.5, 1 and 2 h and the final pyrolysis temperature was chosen as 650 °C, 800 °C and 950 °C. The materials are referred to as SC650, SC800 and SC950 with numbers 0.5, 1 and 2 added to the names to indicate the holding time. After H_2S adsorption E is added to the name of the samples, which refers to the exhausted material.

2.2. Methods

2.2.1. Evaluation of H_2S sorption capacity

A custom-designed dynamic test was used to evaluate the performance of adsorbents for H_2S adsorption from gas streams as described elsewhere [9]. Adsorbent samples were ground, sieved to 1–2 mm particle size, and packed into a glass column (length 370 mm, internal diameter 9 mm, bed volume 6 cm^3), and pre-humidified with moist air (relative humidity 80% at 25 °C) for 1 h. The amount of water adsorbed was estimated from the increase in the sample weight. Moist air (relative humidity 80% at 25 °C) containing 0.3% (3000 ppm) of H_2S was passed through the column of adsorbent at 0.5 L/min. The flow rate was controlled using Cole Palmer flow meters. The breakthrough of H_2S was monitored using electrochemical sensors. The test was stopped at the breakthrough concentration of 350 ppm. The adsorption capacities of each adsorbent in terms of mg of hydrogen sulfide per g of adsorbent were calculated by integration of the area above the breakthrough curves, and from the H_2S concentration in the inlet gas, flow rate, breakthrough time, and mass of sorbent. For each sample the test was repeated at least twice.

2.2.2. Adsorption of nitrogen

On the materials obtained sorption of nitrogen at its boiling point was carried out using ASAP 2010 (Micromeritics). Before the experiments, the samples were outgassed at 120 °C to constant vacuum (10^{-4} Torr). From the isotherms, the surface areas (BET method), total pore volumes, V_t, (from the last point of isotherm at relative pressure equal to 0.99), volumes of micropores, V_{mic}, mesopore volume, V_{mes}, along with pore size distributions were calculated. The last three quantities were calculated using density functional theory, DFT [16,17].

2.2.3. pH

The pH of a carbon sample suspension provides information about the average acidity and basicity of the carbon surface. A sample of 0.4 g of dry carbon powder was added to 20 mL of distilled water and the suspension was stirred overnight to reach equilibrium. Then the pH of suspension was measured.

2.2.4. Thermal analysis

Thermal analysis was carried out using TA Instrument Thermal Analyzer. The instrument settings were: heating rate 10 °C/min and a nitrogen atmosphere with 100 mL/min flow rate. For each measurement about 25 mg of a ground adsorbent sample were used.

2.2.5. SEM

Scanning electron microscopy images were obtained at Zeiss-LEO using LEO 1550 FESEM. Electron Probe Microanalysis (EDX) was performed by CAMEBAX SX-50 Analyser coupled with NORAN Instruments-Voyager detector system. The accelerated voltage was 15 kV. The as received samples were mounted using silver support.

2.2.6. XRF

X-ray fluorescence analysis was applied to study the calcium and iron content in the samples. The SPECTRO model 300T Benchtop Analyzer from ASOMA Instruments, Inc was used. The instrument has a titanium target X-ray tube and a high-resolution detector. The samples were studied in a solid phase after grinding and sieving in order to use the matrices with similar physical properties.

2.2.7. XRD

X-ray diffraction measurements were conducted using standard powder diffraction procedure. Samples were analyzed by Cu Kα radiation generated in a Phillips XRG 300 X-ray diffractometer. A quartz standard slide was run to check for instrument wander and to obtain accurate location of 2θ peaks.

3. Results and discussion

Catalytic performance of the sewage sludge derived materials is summarized in Table 1 as a hydrogen sulfide breakthrough capacity, water adsorption during the prehumidification, and surface pH before and after H_2S adsorption/oxidation. As seen based on the SC650 and SC950 pyrolyzed for half an hour and an 1 h, longer pyrolysis time results in better performance of adsorbents. Also the capacity increases with an increase in the pyrolysis temperature. The surface pH slightly decreases with more severe heating conditions. An increase in heating temperature apparently increases the surface affinity towards water

Table 1
H_2S breakthrough capacity, surface pH, and amount of water preadsorbed

Sample	H_2S breakthrough capacity (mg/g)	Water adsorbed (mg/g)	pH	pHE
SC650-0.5	9	18	10.9	11.1
SC650-1	15	40	11.4	9.2
SC800-1	24	48	11.2	8.8
SC950-0.5	45	26	10.9	10.0
SC950-1	86	62	10.4	9.3
SC950-2	54	32	10.7	9.8

adsorption and an increase in the holding time from half an hour to an hour increases the amount of water adsorbed. On the other hand, too long holding time, as 2 h in the case of SC950-2, has a negative effect on both, the hydrogen sulfide breakthrough capacity and the amount of water preadsorbed.

All the changes mentioned above must be governed by changes in surface chemistry and porous structure. Based on the chemical composition of the sewage sludge used as a precursor [8,9], calcium (20,300 ppm), iron (26,600 ppm), magnesium (5550 ppm), zinc (1290 ppm), aluminum (7410 ppm), copper (932 ppm), sulfur (0.7%), and phosphorus (3.17%) should play a predominant role in chemical transformation and solid state reactions occurring during pyrolysis. Although the DTG analysis of raw sewage sludge indicates that in our temperature range the weight changes are very slight or negligible [8], the reactions between the inorganic/organic components are expecting to take part. XRF analysis shows that an inorganic phase of the final products is especially rich in iron and calcium (Fig. 1).

The X-ray diffraction patterns for samples heated at various temperatures for various times are presented in Figs. 2 and 3. Even the glance at the diffraction patterns clearly demonstrates the differences in the chemistry of materials. Higher temperatures of pyrolysis result in higher degree of mineralization (more sharp peaks) and longer holding times lead to even sharper peaks (Fig. 3). The species detected in our materials are presented in Table 2. It is important to mention that our discussion here is limited only to the materials having well defined crystallographic structures, and other amorphous materials present or those very highly dispersed can be beyond the detection/resolution of the method used.

Based on the mineral phases listed in Table 2, lower pyrolysis temperature results in formation of aluminosilicates with calcium, magnesium and iron as exchangeable cations. Heating at 950 °C leads to the formation of minerals based on zinc, copper, and sulfur. Moreover, the iron salts present at 800 °C (hercynite or almandine) are converted to hematite, Fe_2O_3, or ferroxyhite, FeO(OH) after heating at 950 °C. Also the rare compositions of phosphorus and iron are found. Since calcium and magnesium are present in significant quantity we cannot exclude the presence of amorphous phase of these oxides, which provides basic pH to the system. Examples of the differences in the location of calcium, phosphorus, iron, sulfur, magnesium, aluminum,

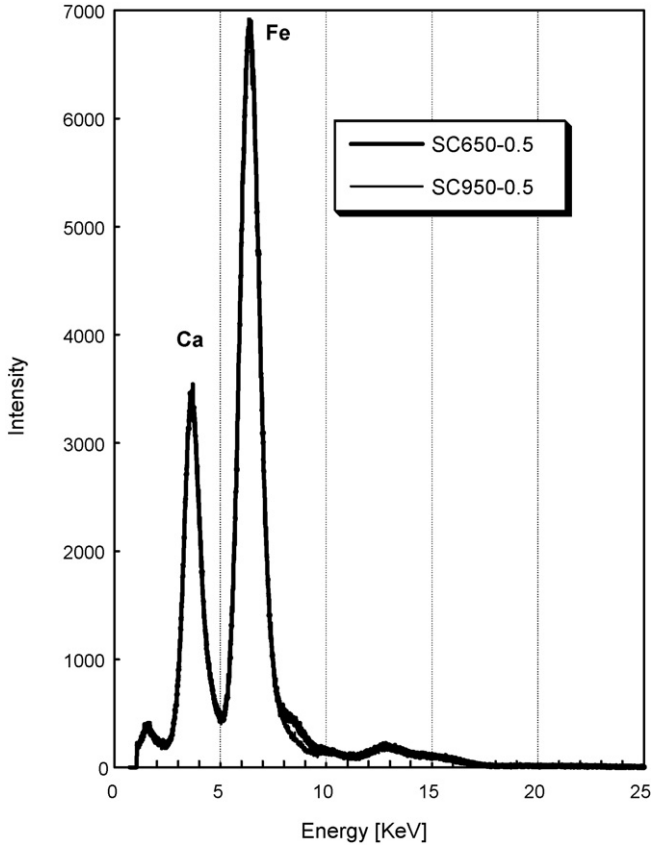

Fig. 1. XRF spectra for SC650-0.5 and SC950-0.5.

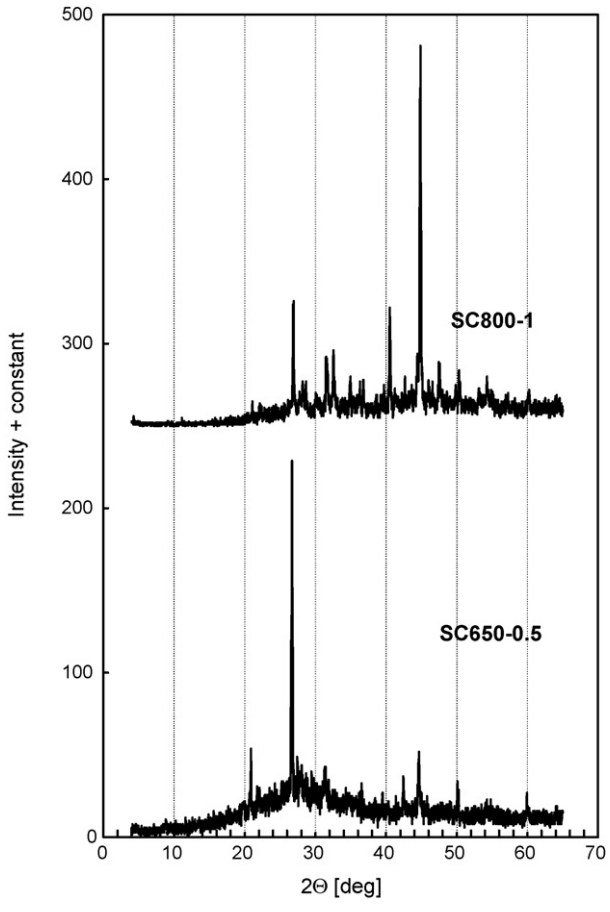

Fig. 2. X-ray diffraction patterns for the samples obtained at 650 °C and 800 °C.

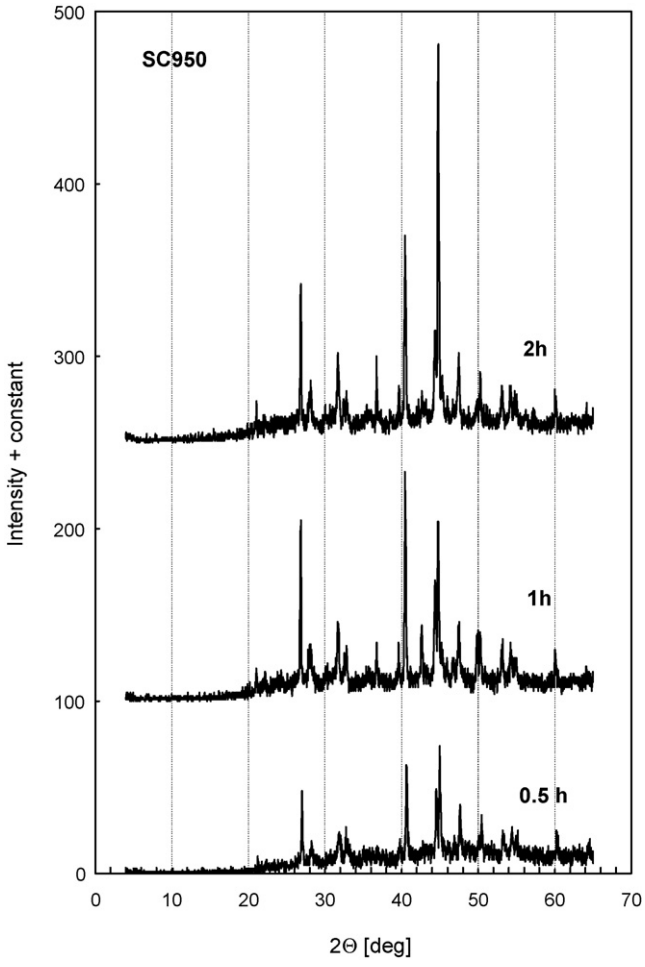

Fig. 3. X-ray diffraction patterns for samples obtained at 950 °C.

and oxygen are presented in Fig. 4 as maps of the elements obtained using EDX [15]. The dispersion of catalytic phase is high since the area scanned is 512 μm × 512 μm. Moreover, as seen from comparison of the initial and exhausted samples, the sulfur deposited on the surface after H_2S adsorption covers it in a very uniformed and homogeneous way indicating the activity of whole surface in the oxidation reactions.

The catalytic surface, to be considered as efficient in the reactive adsorption, has to provide a sufficient pore volume where reaction can occur and product of oxidation can be stored. Analysis of the structural parameters summarized in Table 3 reveals that the differences in the pore structure, however small, show a consistent trend. With an increase in the pyrolysis temperature the surface area and the total pore volume increase while holding the same temperature for various times decreases the structural parameters. Taking into account the nature of the precursor (only about 20% of carbon phase), the majority of the volume of pores in our materials, and thus the surface area accessible to nitrogen molecules, exist either between the particles of inorganic phase (meso- and macropores) or in the interface between carbon and inorganic phase (micro- and mesopores).

After H_2S adsorption, the general trend of a decrease in the volume of pores is noticed for all samples with a marked decrease particularly in the volume of micropores (Fig. 5). These pores either are active in oxidation since adsorption of H_2S and water is enhanced there or sulfur formed on inorganic catalytic centers migrates to these neighborhood high-energy storage places [13]. Another possible scenario is the blockage of the pore entrances for nitrogen by sulfur/sulfides/ sulfites formed at their entrances.

It is interesting that in some cases a significant increase in the volume of small mesopores is found after H_2S adsorption. This likely happens as a result of the deposition of elemental sulfur and sulfides on the catalytically active surface of large pores. In this way the secondary pore network is formed as clearly seen for SC950-0.5E. This secondary pore network may only exist when the parent pores are big enough and when sufficient quantity of amorphous sulfur is deposited within the pore.

To further investigate surface nanotexture, SEM and TEM images were taken for SC800-1 and SC950-1. The former are presented in Fig. 6. The striking features on these micrographs are the presence of needle-like structures [18], which are especially, abundant for the samples obtained in 800 °C. Their size is estimated to be about 15 nm. They seem to grow from some kind of inorganic active centers (Fig. 7). In the case of SC950-1 we can even see the irregular piece of metal at the top of the tubular entities resembling carbon nanotubes. Some of them are in the forms of bundles (Fig. 7), some are even bended as the SEM image shows for SC950. Their sizes are in the range between 20 nm and 50 nm. Another important feature are very regular crystals of an inorganic phase present on the surface with sizes between 20 nm and 200 nm (Fig. 8). They are well dispersed within the amorphous-looking main phase of the material. Taking into account the XRD and EDX results, composition of the materials, and shape of the crystals they probably represent wurtzite.

TEM images suggest that tubular species so clearly seen on SEM images are multiwall carbon nanotubes (MCN) and/or carbon fibers/nanowires. The detection of such carbon entities using transmission electron microscopy is extremely difficult on our materials due to their location on a surface of the inorganic support, often perpendicular or parallel to it (Fig. 6). Some of the tubes are open, some closed and some form agglomerates close to the catalytic center of their growth. Their diameters are between 20 nm and 50 nm and with length of between few hundred nanometers and a micron, which is in agreement with the SEM analysis. As mentioned above, they grow on the well-dispersed inorganic particles with sizes of about 20–200 nm present within the amorphous carbon and seen in TEM micrographs as black particles (white hexagonal crystals seen on SEM images).

The difference between SC800-1 and SC950-1 is definitely in the density and length of the nanotubes present. More nanotubes in the case of the former sample is the result of the differences in the chemical composition. The catalytic centers for nanotubes formation in our case are likely small particles of iron highly dispersed on the surface [19], since iron is one of the main catalytic components of our samples [8,9]. These small particles cannot be detected as a separate crystallographic phase in XRD analysis. Indeed, the crystals of metallic iron were detected in the samples pyrolized at 950 °C but not at those obtained at 800 °C. Besides iron, also other catalytic metals, known as active in nan-

Table 2
Mineral phases detected from XRD analysis

SC650-0.5	SC800-1	SC950-0.5	SC950-1	SC950-2
Aluminium Al	Aluminium Al			Aluminium Al
Iron Fe			Iron Fe Fersilicite FeSi	Iron Fe
		Bornite Cu_5FeS_4 Spinel $MgAl_2O_4$	Bornite Cu_5FeS_4	Bornite Cu_5FeS_4
			Hematyte Fe_2O_3	
	Hibonite $CaAl_{12}O_{19}$ Hercynite $FeAl_2O_4$			
Calcite $CaCO_3$	Huntite $Mg_3Ca(CO_3)_4$		Vaterite $CaCO_3$	
Sapphirine $(Mg_4Al_4)Al_4Si_2O_{20}$				Sapphirine $(Mg_4Al_4)Al_4Si_2O_{20}$
	Pyrope $Mg_3Al_2(SiO_4)_3$			
			Barringerite Fe_2P	Barringerite Fe_2P
	Wurtzite ZnS	Wurtzite ZnS Ferroxyhite, goethite FeO(OH)		Sphalerite/wurtzite ZnS
	Almandine $Fe_3Al_2(SiO_4)_3$			
Quartz, Cristobalite SiO_2		Quartz SiO_2	Quartz SiO_2	

otube formation, such as nickel exist in our materials, however their content is much smaller then that of iron (5.6% of iron).

Although formation of nanotubes does not seem to have an apparent effect on H_2S adsorption/oxidation, it has to be mentioned here that the capacity of materials obtained at 800 °C is much higher than those obtained at 650 °C (24 mg/g compared to 15 mg/g). It is well known that temperature of 650 °C, however high enough for carbonization, is not sufficiently high for formation of nanotubes via carbon diffusion in metal particle [20]. Moreover, removal of an active inorganic phase by acid washing from samples leads to about 10% higher capacity for the sample obtained at 800 °C in comparison with that at 950 °C (acid washed), which might be related to higher density of nanotubes present on the surface of this material (Fig. 6). When the most active inorganic centers are removed via acid washing, the surface texture plays more important role in adsorption.

Table 3
Structural parameters calculated from nitrogen adsorption isotherms

Sample	S_{BET} (m^2/g)	V_{mic} (cm^3/g)	V_{mes} (cm^3/g)	V_t (cm^3/g)	V_{mes}/V_t
SC650-0.5	92	0.037	0.076	0.113	67
SC650-0.5E	79	0.029	0.077	0.106	73
SC650-1	99	0.030	0.085	0.115	76
SC650-1E	14	0.001	0.039	0.040	99
SC800-1	104	0.033	0.074	0.107	69
SC800-1E	14	0.003	0.063	0.064	99
SC950-0.5	141	0.058	0.151	0.209	72
SC950-0.5E	121	0.032	0.190	0.222	86
SC950-1	125	0.048	0.139	0.187	74
SC950-1E	47	0.018	0.114	0.132	86
SC950-2	115	0.048	0.112	0.160	70
SC950-2E	30	0.011	0.084	0.095	88

Since chemistry of the surface is without any doubt the main factor governing the removal of hydrogen sulfide, its effect on immobilization/oxidation reactions should be revisited in details. Fig. 9 shows the DTG curves for samples before and after H_2S adsorption. The peaks on the DTG curves for the exhausted samples represent the removal of oxidation products. Since the pH values of the adsorbents were not changed significantly (Tables 1 and 4) after removal of hydrogen sulfide, the main products of oxidation are elemental sulfur, sulfides, sulfates and sulfites. The two latter can be formed from sulfides via their oxidation with oxygen or via reactions of acids with oxides of the surface, especially the alkaline earth oxides present in our materials in a significant quantity. If, as shown previously [10], we assume that the peak between 150 °C and 400 °C represents removal of elemental sulfur from large pores and the amount of sulfur represented by that peak is compared

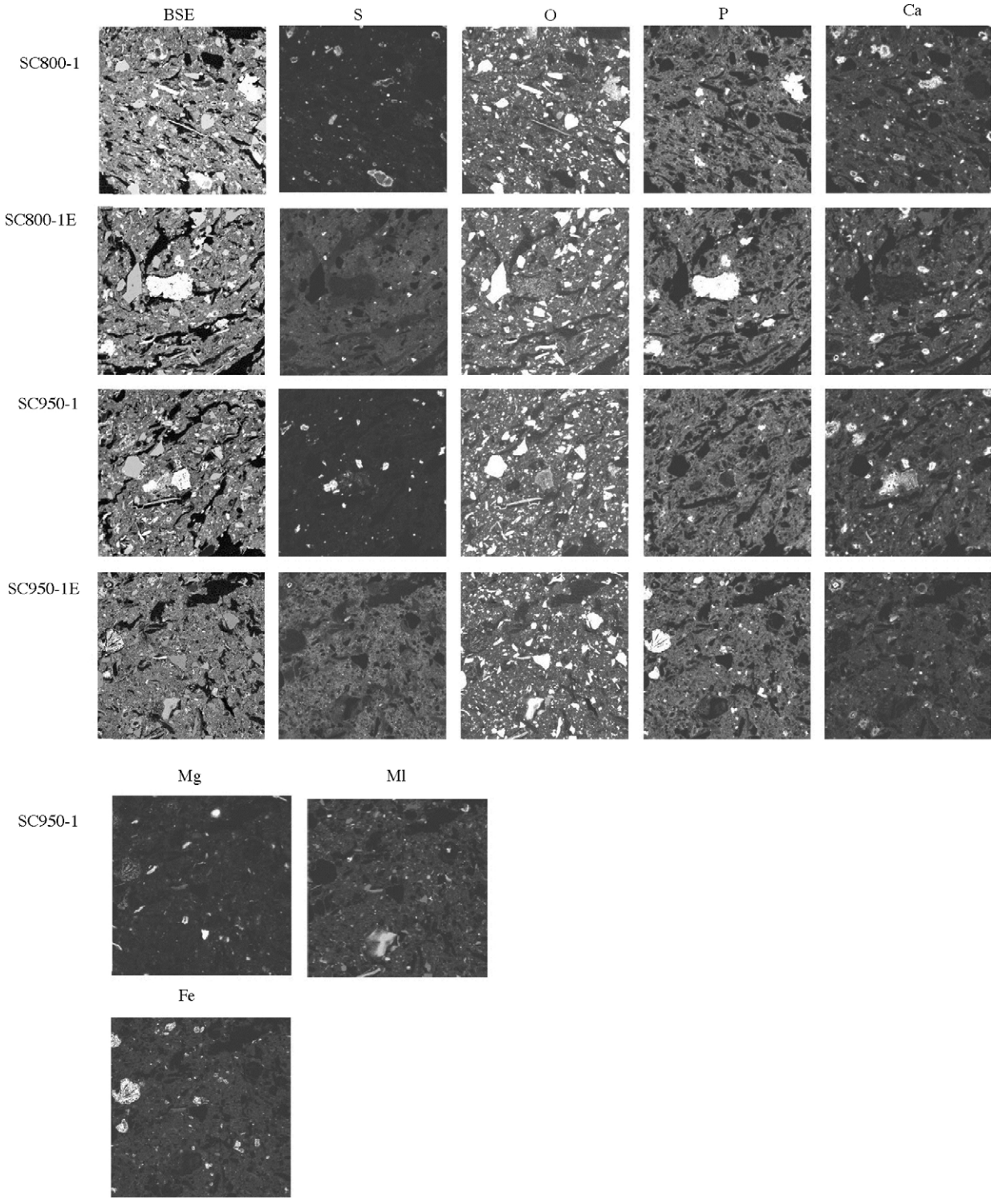

Fig. 4. EDX maps of elements.

to the total amount of sulfur expected on the surface based on the breakthrough experiments, the selectivity for oxidation to elemental sulfur can be calculated (Table 4). It is important to mention that to calculate these amounts, the differences between the initial and exhausted samples have to be taken into account along with the correction for the weight increase for the samples obtained at 950 °C (negative peaks on DTG curves). That weight increase, referred to as $\Delta\Omega$ in Table 4, is difficult to explain since the samples were obtained at high temperature and during the experiments were exposed to pure nitrogen. Nitride formation, although reported even at 110 °C [20] and possible at higher temperatures (about 1000 °C) in the presence of char [21,22] does not seem to be a very plausible scenario. Nevertheless, this interesting phenomenon of weight increase is registered only for

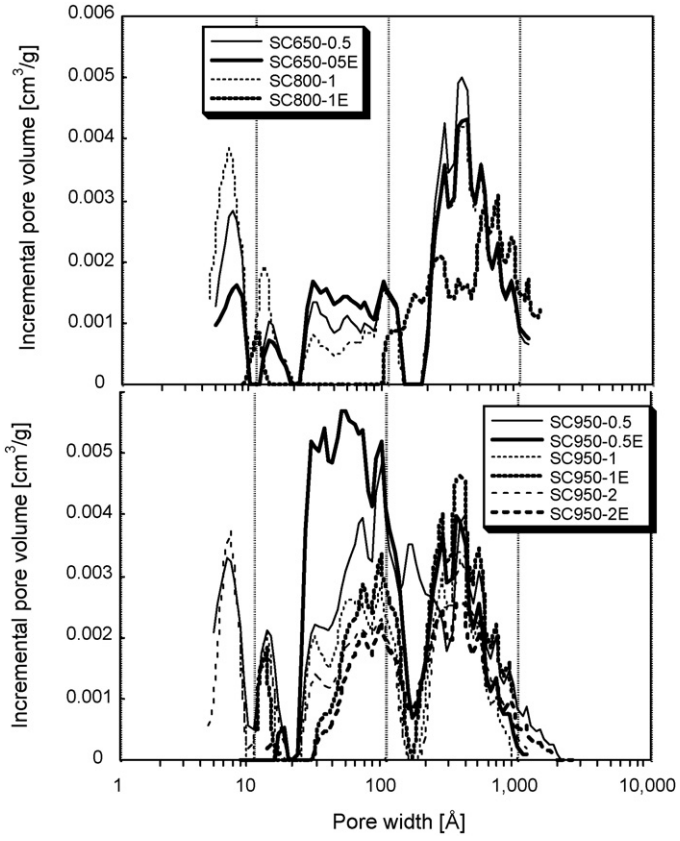

Fig. 5. Pore size distributions for samples before and after H_2S adsorption.

Table 4
Decrease in the pH − ΔpH, amount of sulfur expected based on the H_2S breakthrough capacity

Sample	ΔpH	S_{BT} (%)	ΔW (%)	$\Delta\Omega$ (%)	S_{el} (%)	ΔV_{mic} (%)
SC650-0.5	0	0.8	0.15	–	19	22
SC650-1	1.8	1.3	0.46	–	35	97
SC800-1	2.4	2.2	0.58	–	26	91
SC950-0.5	0.9	4.2	2.02	0.95	48	45
SC950-1	1.1	8.1	4.32	0.82	53	62
SC950-2	0.9	5.2	1.99	0.07	38	73

S_{BT}, effective weight loss between 150 °C and 400 °C, ΔW, weight increase for initial samples between 150 °C and 400 °C, $\Delta\Omega$, selectivity for oxidation to elemental sulfur, S_{el}, and a decrease in the volume of micropores after H_2S adsorption, ΔV_{mic}.

the most catalytically active samples, SC950. One would expect those samples to be the most stable since they were pyrolized at the highest temperature.

Analysis of the data presented in Table 4 and DTG curves in Fig. 9 shows differences in catalytic activities of the samples. The selectivity for oxidation to elemental sulfur ranges from 20–55%. It increases with an increase in pyrolysis temperature and, for the same temperature, with pyrolysis time, however a maximum in activity is observed for SC950-1. Over two units decrease in the pH of SC800-1 indicates the formation of weak acids or amphiprotic salts on its surface. On the other hand, the pH for SC650-0.5 slightly increases while the pH for SC950 samples decreases one unit in spite of the differences in the pyrolysis time. These changes are caused by various mechanisms of the hydrogen sulfide oxidation reactions.

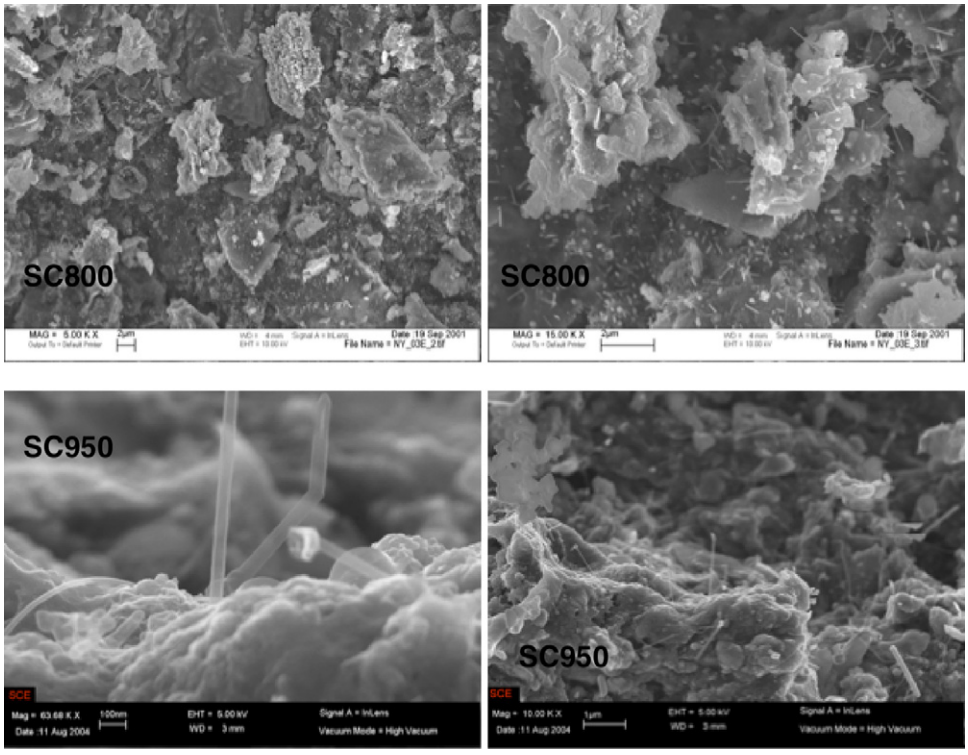

Fig. 6. SEM images for the samples pyrolized at 800 °C and 950 °C.

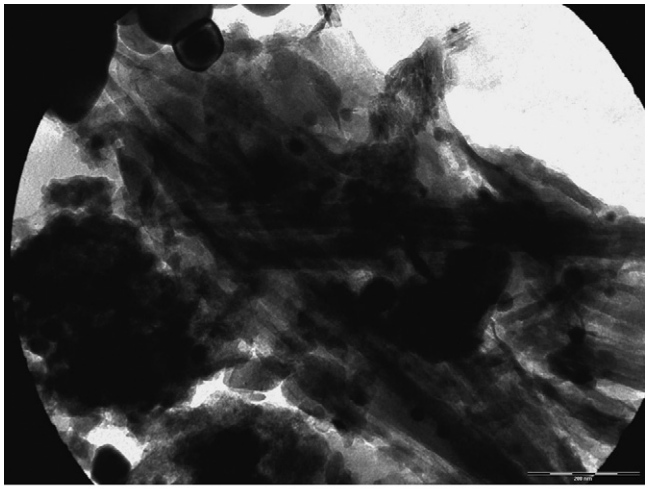

SC800-1

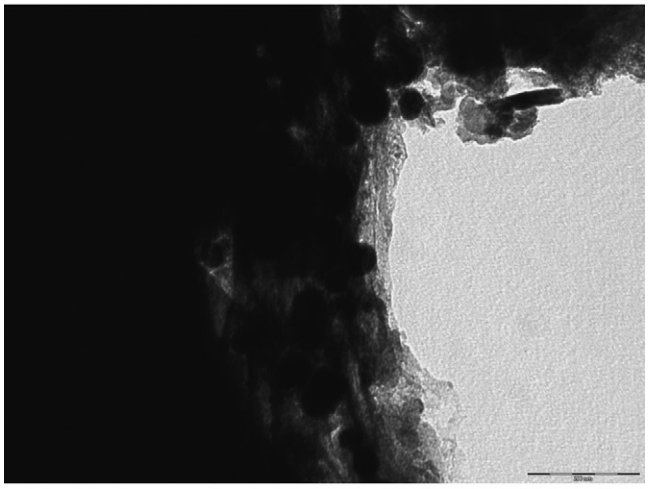

SC950-1

Fig. 7. TEM images for the samples pyrolized at 800 °C and 950 °C. The magnification bars represent 200 nm.

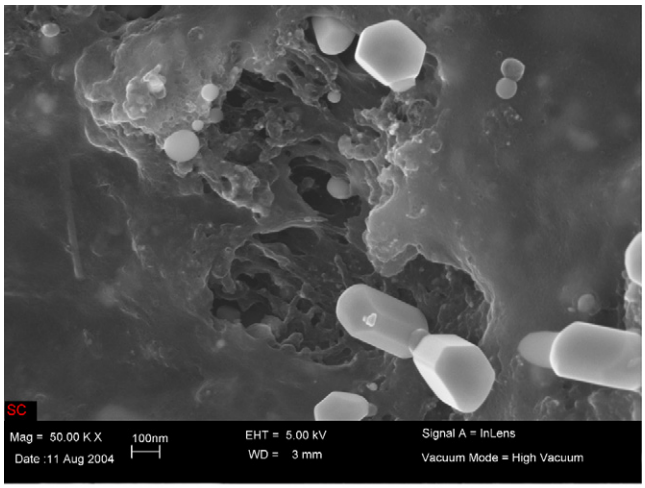

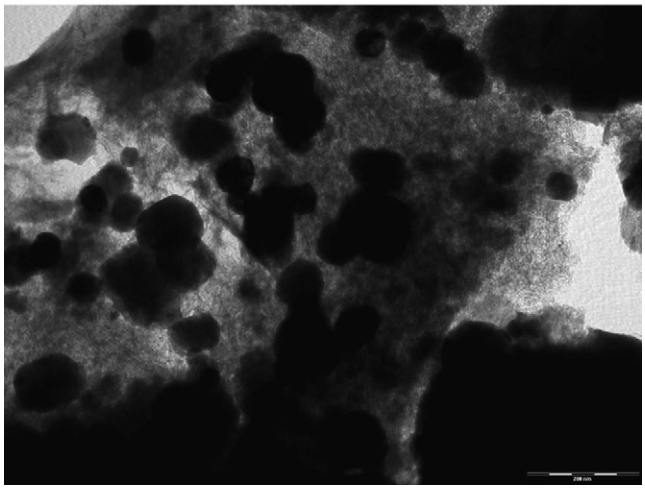

Fig. 8. Inorganic and organic phases on SEM and TEM images of SC950-1.

In the case of SC650-0.5 whose surface is expected to have amorphous calcium and magnesium oxides, which cause the most basic pH of this material in the presence of water, the following reactions can occur (with calcium and magnesium):

$$CaO + H_2O \rightarrow Ca(OH)_2 \quad (1)$$

$$Ca(OH)_2 + 2H_2S \rightarrow Ca(HS)_2 + 2H_2O \quad (2)$$

$$Ca(HS)_2 + O_2 \rightarrow 2S + Ca(OH)_2 \quad (3)$$

Besides this, many cations are present in the forms of salts and their sulfides are formed. They decompose at temperatures higher than 1000 °C [23]. Sulfide formation must be the predominant hydrogen sulfide removal mechanism in the case of SC650.

For SC800-1, magnesium and calcium in hibonite, huntite and pyrope and iron in hecynite or almandine can bond sulfur and form sulfides. Those sulfides can be further oxidized to sulfites by oxygen from air since the breakthrough capacity (time) is relatively high. This leads to the decrease in the surface pH. Oxidation of sulfides at the entrances of small pores can block those pores for nitrogen molecules. As seen from Table 4, also elemental sulfur is formed in small quantity on SC-800 and the mechanism should be similar to that on SC650.

Pyrolyzing samples at 950 °C results in formation of reactive redox catalysts such as FeO(OH) and Fe_2O_3. They presence promotes the following oxidation reactions:

$$FeO(OH) + HS^- \rightarrow FeO + S + H_2O \quad (4)$$

$$Fe_2O_3 + 2HS^- \rightarrow 2FeO + H_2O + 2S \quad (5)$$

Ferrous oxide can be further oxidized to ferric oxide by oxygen from air. Reaction (5) is much more efficient in formation of sulfur than reaction (4), which explains why the capacity of SC950-1 is found to be the biggest and the selectivity for oxidation to elemental sulfur—the highest. The decrease in catalytic activity in the case of SC-950-2 can be caused by reduction of Fe_2O_3 to elemental iron when the sample is exposed to high temperature for long time.

Proposing the reaction mechanisms on the sludge derived materials one has to keep in mind that all of them are oversimplified. In these materials many various minerals/catalytic compounds are present and they certainly contribute to their excellent performance in the process of hydrogen sulfide oxidation. Unfortunately, at this stage of our study, and due to the

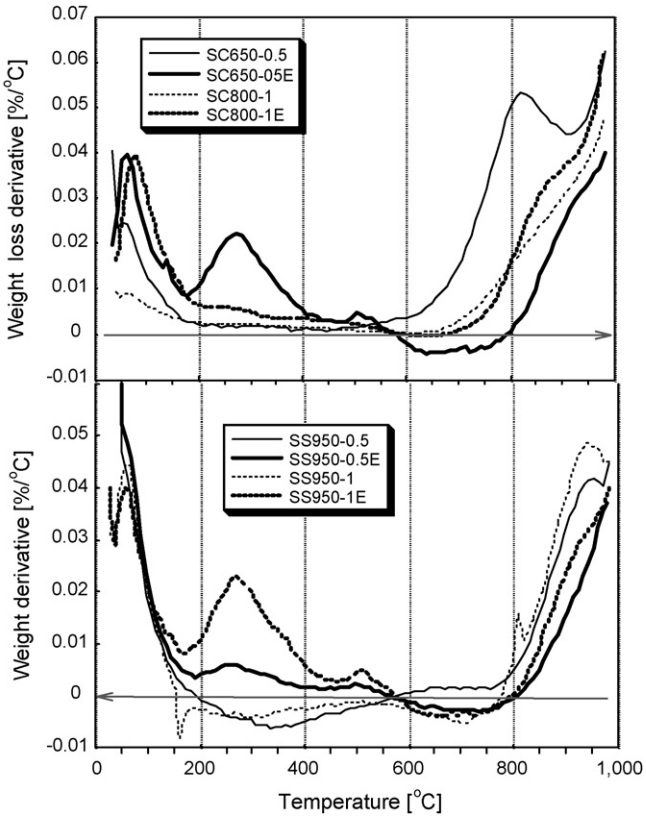

Fig. 9. DTG curves in nitrogen for samples before and after H_2S adsorption.

complexity of the chemistry of the precursor, we are not able to identify without any doubt other species governing reactive adsorption of H_2S.

4. Conclusions

Summarizing, the results presented in this paper provide evidence that complex waste products such as sludges may be used as precursors for composite catalytic materials with sophisticated nano-features. After thermal treatment their surface represents the mixture of carbon nanostructures, and an active inorganic phase, highly dispersed within the surface layer of amorphous carbon. Important aspects of pyrolysis, which can be used as factors tailoring the catalytic properties are the temperature of heat treatment and exposure time. They are crucial for formations of catalytic phases via solid state reactions. The mechanism of nanotube formation can be referred as self-imposed chemical vapor deposition-SICVD. All the important components for CNT deposition (organic source of carbon and well dispersed catalysts) are already present in the initial materials.

Acknowledgements

We are grateful to Dr. Boris Reznik of University of Karlsrue, Dr. David Frey of Zeiss and Dr. Jorge Morales of CCNY for their involvements in obtaining the presented SEM and TEM images. The contribution of Ms. Karin Block to performing X-ray analysis is highly appreciated.

References

[1] J. Lee, K. Sohn, T.J. Hyeon, Am. Chem. Soc. 123 (2001) 5146–5147.
[2] Z. Wang, R. Bai, Ind. Eng. Chem. Res. 44 (2005) 825–831.
[3] D. Nguyen-Tanh, T.J. Bandosz, Carbon 43 (2005) 359–367.
[4] R. Leboda, B. Charmas, J. Skubiszewska-Zieba, S. Chodorowski, P. Oleszczuk, V.M. Gun'ko, V.A. Pokrovskiy, J. Coll. Interf. Sci. 248 (2005) 39–47.
[5] J.R. Kastner, K.C. Das, Q. Buquoi, N.D. Melear, Environ. Sci. Technol. 37 (2003) 2568–2574.
[6] J.R. Kastner, K.C. Das, N.D. Melear, J. Haz. Mat. B95 (2002) 81–90.
[7] A. Bagreev, D.C. Locke, T.J. Bandosz, Carbon 39 (2001) 1971–1978.
[8] A. Bagreev, S. Bashkova, D.C. Locke, T.J. Bandosz, Environ. Sci. Technol. 35 (2001) 1537–2143.
[9] A. Bagreev, S. Bashkova, T.J. Bandosz, Environ. Sci. Technol. 38 (2004) 345–351.
[10] A. Ansari, A. Bagreev, T.J. Bandosz, Carbon 43 (2005) 359–367.
[11] A. Ansari, T.J. Bandosz, Environ. Sci. Technol. 39 (2005) 6217–6622.
[12] E. Sioukri, T.J. Bandosz, Environ. Sci. Technol. 39 (2005) 6225–6230.
[13] A. Bagreev, T.J. Bandosz, Ind. Chem. Eng. Res. 44 (2005) 530–538.
[14] Graham, J. US Patent 6,858,192 (2005).
[15] A. Bagreev, T.J. Bandosz, Environ. Sci. Technol. 38 (2004) 345–351.
[16] Ch. Lastoskie, K.E. Gubbins, N. Quirke, J. Phys. Chem. 97 (1993) 4786–4796.
[17] J.P. Olivier, J. Porous Mater. 2 (1995) 9.
[18] A. Bagreev, S. Bashkova, B. Reznik, V. Zibat, T.J. Bandosz, in: F. Rodriguez-Reinoso, et al. (Eds.), Proceeding of the Conference on Characterization of Porous Solids-6 (Studies in Surface Science and Catalysis 144), Elsevier, Amsterdam, 2003, pp. 217–224.
[19] M.S. Dresselhaus, G. Dreselhaus, P.C. Eklund, Science of Fulerenes and Carbon Nanotubes, Academic Press, San Diego, CA, 1996.
[20] X.P. Hao, M.Y. Yu, D.L. Cuo, X.G. Xu, Y.J. Bai, Q.L. Wang, M.H. Jiang, J. Crystal Growth 242 (2002) 229–232.
[21] O. Yamamoto, M. Ishida, Y. Saitoh, T. Sasamoto, S. Shimada, Inter. J. Inorg. Mat. 3 (2001) 715–719.
[22] R. Koc, S.J. Kaza, Euro. Ceram. Soc. 18 (1998) 1471–1477.
[23] R.C. Weast (Ed.), Handbook of Chemistry and Physics, 67th ed., CRC Press, Boca Raton, FL, 1986.